

RESEARCH

Open Access



Quercetin inhibits SARS-CoV-2 infection and prevents syncytium formation by cells co-expressing the viral spike protein and human ACE2

Annie V. Roy¹, Michael Chan², Logan Banadyga^{2,3}, Shihua He², Wenjun Zhu^{2,4}, Michel Chrétien¹ and Majambu Mbikay^{1*}

Abstract

Background Several *in silico* studies have determined that quercetin, a plant flavonol, could bind with strong affinity and low free energy to SARS-CoV-2 proteins involved in viral entry and replication, suggesting it could block infection of human cells by the virus. In the present study, we examined the *ex vivo* ability of quercetin to inhibit of SARS-CoV-2 replication and explored the mechanisms of this inhibition.

Methods Green monkey kidney Vero E6 cells and in human colon carcinoma Caco-2 cells were infected with SARS-CoV-2 and incubated in presence of quercetin; the amount of replicated viral RNA was measured in spent media by RT-qPCR. Since the formation of syncytia is a mechanism of SARS-CoV-2 propagation, a syncytialization model was set up using human embryonic kidney HEK293 co-expressing SARS-CoV-2 Spike (S) protein and human angiotensin converting enzyme 2 (ACE2), [HEK293(S + ACE2) cells], to assess the effect of quercetin on this cytopathic event by microscopic imaging and protein immunoblotting.

Results Quercetin inhibited SARS-CoV-2 replication in Vero E6 cells and Caco-2 cells in a concentration-dependent manner with a half inhibitory concentration (IC₅₀) of 166.6 and 145.2 μM, respectively. It also inhibited syncytialization of HEK293(S + ACE2) cells with an IC₅₀ of 156.7 μM. Spike and ACE2 co-expression was associated with decreased expression, increased proteolytic processing of the S protein, and diminished production of the fusogenic S2' fragment of S. Furin, a proposed protease for this processing, was inhibited by quercetin *in vitro* with an IC₅₀ of 116 μM.

Conclusion These findings suggest that at low 3-digit micromolar concentrations of quercetin could impair SARS-CoV-2 infection of human cells partly by blocking the fusion process that promotes its propagation.

Keywords Quercetin, SARS-CoV-2, Spike protein, Human ACE2, HEK293 cells, Syncytium formation

*Correspondence:

Majambu Mbikay
majambu.mbikay@ircm.qc.ca

¹Functional Endoproteolysis Laboratory, Montreal Clinical Research Institute, Montreal, QC, Canada

²Special Pathogens Program, National Microbiology Laboratory, Public Health Agency of Canada, Winnipeg, MB, Canada

³Department of Medical Microbiology and Infectious Diseases, University of Manitoba, Winnipeg, MB, Canada

⁴National Centre for Foreign Animal Disease, Canadian Food Inspection Agency, Winnipeg, MB, Canada



© The Author(s) 2024. **Open Access** This article is licensed under a Creative Commons Attribution 4.0 International License, which permits use, sharing, adaptation, distribution and reproduction in any medium or format, as long as you give appropriate credit to the original author(s) and the source, provide a link to the Creative Commons licence, and indicate if changes were made. The images or other third party material in this article are included in the article's Creative Commons licence, unless indicated otherwise in a credit line to the material. If material is not included in the article's Creative Commons licence and your intended use is not permitted by statutory regulation or exceeds the permitted use, you will need to obtain permission directly from the copyright holder. To view a copy of this licence, visit <http://creativecommons.org/licenses/by/4.0/>. The Creative Commons Public Domain Dedication waiver (<http://creativecommons.org/publicdomain/zero/1.0/>) applies to the data made available in this article, unless otherwise stated in a credit line to the data.

Background

Severe Acute Respiratory Coronavirus 2 (SARS-CoV-2) is the etiological agent of coronavirus disease 2019 (COVID-19) that broke out in 2019 in China before becoming a pandemic that has killed to date nearly 15 million people worldwide [1]. SARS-CoV-2 primarily infects epithelial cells of respiratory airways where it multiplies, releasing virions that disseminate to other organs including heart, liver, bowel, kidney, and brain. Infection by the virus often elicits from the host an inflammatory response that can evolve into a potentially fatal “cytokine storm”. The most common symptoms of COVID-19 include fever, cough, fatigue, anosmia and ageusia; common symptoms include pharyngitis, cephalgia, myalgia, iritis, or diarrhea; complications include dyspnea, pneumonia, severe acute respiratory distress syndrome, hypercoagulation syndrome, and multiple organ failure [2]. The global case fatality rate of COVID-19 was estimated at 8.5% in February 2020; it had decreased to 0.27% by August 2022 [3]. It comprises, for a large part, the elderly and individuals with preexisting morbidities such as chronic obstructive pulmonary disease, coronary heart disease, diabetes mellitus, and hypertension [4, 5].

SARS-CoV-2 entry into cells begins with the binding of the viral Spike (S) protein to human angiotensin converting enzyme 2 (ACE2), followed by the proteolytic cleavage of S by furin into the S1 ectodomain and the S2 transmembrane domain. Further cleavage of the S2 fragment by either furin or transmembrane protease serine 2 (TMPRSS2) exposes the fusion peptide at the amino terminus of the transmembrane S2' domain, initiating the fusion of the viral envelope to the cell plasma membrane and the entry of the virus into the cell. In cellular lysosomes, the virus is unpacked into its RNA and protein components, a process facilitated by cathepsins B and L (CatB and CatL); the RNA is translated into a polyprotein which is cleaved by viral main protease (M^{pro}), papain-like protease (PL^{pro}), and 3 chymotrypsin-like protease ($3CL^{pro}$) to generate functional proteins; the RNA is replicated by viral RNA-dependent RNA polymerase (RdRp); the new RNA is translated to produce new proteins; these RNA and proteins are assembled into virions which are released in the extracellular milieu [2].

Proteins that facilitate viral entry and replication are potential targets for inhibition of SARS-CoV-2 infection. Viral entry can be interfered with by blocking the binding of S protein to ACE2 using either soluble decoy ACE2 or anti-S antibodies. RNA or protein vaccines eliciting endogenous anti-S neutralizing antibodies have been approved by regulatory agencies after conclusive clinical trials. Their use in mass immunization of populations around the world has gone a long way in controlling the COVID-19 pandemic by reducing its severity and lethality [6]. Besides these prophylactic measures, potential

therapeutic drugs targeting various enzymes in the viral life cycle have been investigated, among them inhibitors of TMPRSS2 (e.g. camostat) [7, 8], cathepsins (e.g. hydroxychloroquine) [9, 10], $3CL^{pro}$ (e.g. ritanovir, nirmatrelvir) [11], and RdRp (e.g. remdesivir) [12, 13]. Paxlovid, a combination of ritanovir and nirmatrelvir, is now an approved oral drug against early stages of COVID-19 [14].

Interestingly, quercetin, a plant flavonol, could also be an anti-COVID-19 drug. Indeed, molecular docking analyses have indicated that it can bind with relatively strong affinity to several SARS-CoV-2 proteins including S protein, $3CL^{pro}$, and RdRp [15], as well as to cellular ACE2 [16] and TMPRSS2 [17]. Moreover, it has been shown to inhibit to varying degrees the in vitro enzymatic activities of furin [18], ACE2 [19], $3CL^{pro}$ [20], M^{pro} [21], and RdRp [22]. Besides these possible interferences with the infection by SARS-CoV-2, quercetin is also likely to attenuate COVID-19 through its recognized potent antioxidant and anti-inflammatory properties [23], since oxidative stress and inflammation are prominent features of the pathophysiology of the disease [24].

Despite these promising indications, very few studies have experimentally explored the activities of quercetin against SARS-CoV-2 infection. Here we report that, at low 3-digit micromolar concentrations, this flavonol reduced SARS-CoV-2 replication in Vero E6 and Caco-2 cells. Furthermore, using syncytium formation by HEK293 cells co-expressing the viral S protein and human ACE2 as a surrogate model for the cytopathic effect that follows SARS-CoV-2 infection, we show that, at viral replication-inhibiting concentrations, quercetin prevented syncytium formation, presumably by decreasing the proteolytic conversion of the S protein to the fusogenic S2' fragment.

Methods

Reagents

Uncommon reagents, their commercial sources and catalog numbers are presented in Supplementary Table S1.

Cell culture

African green monkey kidney Vero E6 cells and human embryonic kidney 293 (HEK293) cells were cultured in Dulbecco's Modified Eagle Medium (DMEM) supplemented with 10% heat-inactivated fetal bovine serum (hiFBS), 1% L-Glutamine, and 1% penicillin/streptomycin (PeniStrept). Human colon carcinoma Caco2 cells were cultured in Minimal Essential Medium (MEM) containing the same supplements as described for Vero E6 cells. These cell culture media are hereafter referred to as complete media. All cells were cultured at 37 °C in a 5% CO₂ atmosphere.

SARS-CoV-2 infections of Vero E6 and Caco-2 cells

Quercetin was dissolved in DMSO and then diluted to various concentrations in treatment medium (DMEM or MEM, plus 2% hiFBS, 1% L-Glutamine, 1% PeniStrept). VeroE6 and Caco2 cells were cultured in triplicate in 24-well plates in complete medium. When the cells reached 80–90% confluency, medium was removed and replaced with 500 μ l treatment medium. Following a 1 h incubation, cells were infected by addition of 250 μ l of medium containing SARS-CoV-2/Canada/ON-VIDO492 01/2020 (GISAID accession # EPI_ISL_425177) for a multiplicity of infection (MOI) of 0.1. The final concentrations of quercetin in each replicate were 6.25, 12.5, 25, 50, 100, 200, 400, and 800 μ M, and the final concentration of DMSO was 0.3% v/v. Control cells were treated with an equivalent volume of treatment medium containing 0.3% v/v DMSO but no quercetin. Cells were incubated at 37 °C in a 5% CO₂ for 48 h before supernatant was harvested for the quantification of viral RNA.

For quantification of infectious SARS-CoV-2, Vero E6 cells were seeded in 96-well plate such that confluency was ~95% the following day; supernatants from two independent drug treatment studies (performed on both Vero E6 and Caco2 cells) were serially diluted 10-fold in DMEM containing 2% hiFBS and 1% L-glutamine, and 100 μ l of each dilution was used to inoculate cells in triplicate; cells were incubated at 37 °C and 5% CO₂ for seven days, after which they were assessed for cytopathic effect (CPE). The median tissue culture infectious dose (TCID₅₀) per ml was calculated for each supernatant sample using the Reed and Muench method. Because the highest concentration (800 μ M) of quercetin used in Caco2 cells resulted in CPE in one of three wells at the lowest dilution used (10–1), we were unable to calculate the TCID₅₀ for this sample. Instead, the sample was assigned the value of the limit of detection, which was calculated by assuming that a 100 dilution would have produced three of three wells with CPE.

All work with infectious virus was performed in the containment level 3 (CL-3) facility at the National Microbiology Laboratory (NML) of the Public Health Agency of Canada (PHAC) in the Canadian Science Centre for Human and Animal Health (CSCHAH), Winnipeg, Canada. All procedures were conducted in accordance with standard operating protocols appropriate for this level of biosafety.

Transfection of HEK293 cells

Expression vectors include the following plasmids: (i) pEGFP-C1 for expression eGFP (hereafter abbreviated as pGFP); (ii) pcDNA3.1-hACE2-C9 for expression of human ACE2 with a C9 tag at its C-terminus (hereafter abbreviated as pACE2); (iii) 2019-nCov-Linker_pcDNA3.1(+)-C-eGFP for expression of the SARS-CoV-2

spike protein fused through a linker peptide to a C-terminal enhanced green fluorescent protein (eGFP) (hereafter abbreviated as pS-GFP); (iv) 2019-nCov_pcDNA3.1(+)-P2A-eGFP for separate expression the Spike protein and the eGFP (hereafter abbreviated as pS-P2A-GFP). A P2A peptide placed immediately upstream of a glycine causes the ribosome to skip the formation of a peptide bond between the glycine and the next amino acid [25], allowing Spike and eGFP to be translated at the same time but as two unfused proteins. Most experiments were conducted with two expression vectors. When a single expression vector was used, pcDNA-3 was supplemented as an empty vector (EV) to equalize the amount of transfected DNA.

Plasmid transfection was conducted using jetPRIME® Transfection Reagent per manufacturer's protocol. Transfection vectors were either a 1:1 mix of pACE2 and pS-GFP, a 1:1 mix of pACE2 and pGFP, or 1:1 mix of pS-GFP and pcDNA3 as EV. In a typical experiment, cells were cultured in complete medium as monolayers in 96-well plates; spent media was removed and replaced with 100 μ l/well of a 1:9 mixture of jetPRIME® and complete medium. After a 4-h incubation, the transfection medium was removed; cell monolayers were rinsed with complete medium; they were then supplemented with complete medium containing 0.2% DMSO (control) or varying micromolar concentrations of quercetin and 0.2% DMSO; they were further incubated for 16 h.

IncuCyte capture of syncytium formation and fluorescence

Cells were seeded onto 96-well black/clear bottom plates (Corning) at a density of 30,000 cells/well in triplicates for each condition. After a 24-h incubation, they were transfected, processed, and treated as described above under "Transfection of HEK293 cells". The IncuCyte® S3 Live-Cell Analysis System (Essen BioScience) was used to capture images of eGFP-emitted fluorescence from each well every 4 h for up to 48 h with a 4 \times objective, a Green/Red 4614 optic module, and 300 ms exposure. Syncytialization inhibition was accompanied by a decrease in fluorescence. To determine the half inhibitory concentration (IC₅₀) of quercetin on syncytium formation, integrated intensity of fluorescence [Green Calibrated Unit (GCU) \times μ m²/well] at 20 h post-transfection (16 h post-treatment) was quantified and normalized against that of DMSO-treated control cells.

Confocal microscopy

Transfected HEK293 cells were seeded in an 8-chamber slide at a density of 82 500 cells/chamber and incubated for 24 h. They were fixed with 4% paraformaldehyde for 20 min, washed twice with phosphate buffered saline (PBS), incubated with Hoechst (diluted 1:7500 in PBS) for 10 min to stain DNA, washed again twice, and then

overlaid with 300 μ l of PBS/chamber. Images were acquired using the AxioObserver LSM700 inverted confocal microscope; (Zeiss) with a 20 \times objective and processed using the Zen 3.4 software. Excitation/emission wavelengths were 405/435 nm for Hoechst and 488/518 nm for eGFP. For best localize eGFP fluorescence in synctia, the laser power at 488 nm had to be doubled for HEK293(S+ACE2) cells treated with 0 to 100 μ M quercetin to compensate for the reduced fluorescence due to cell fusion. Images were captured with a resolution of 2048 \times 2048 pixels.

Cell viability assay

Quercetin cytotoxicity was assessed in VeroE6 and Caco2 cells. Quercetin was dissolved in DMSO and then diluted to various concentrations in treatment medium (DMEM or MEM, plus 2% hiFBS, 1% L-Glutamine, 1% PeniStrept). Cells were seeded in triplicate in a 96-well plate. Upon reaching 80–90% confluency, medium was removed and replaced with 100 μ l treatment medium. Following a 1-h incubation at 37 $^{\circ}$ C, an additional 50 μ l of treatment medium was added. The final concentrations of quercetin were 6.25, 12.5, 25, 50, 100, 200, and 400 μ M, and the final concentration of DMSO in each replicate was 0.3% v/v. Control cells were treated with an equivalent volume of treatment medium containing 0.3% v/v DMSO but no quercetin. After 48 h of drug treatment, cells were washed once with PBS, and cell viability was assessed using the CyQUANT™ XTT Cell Viability Assay kit according to manufacturer's directions.

HEK293 cells were seeded in a 96-well plate at a density of 3×10^4 cells/well and incubated for 24 h; the medium was supplemented with DMSO to a final concentration of 0.2% (v/v, controls) or to varying micromolar concentrations of quercetin and final 0.2% DMSO; incubation was resumed for 24 h. Cell viability was measured using the Abcam MTS Cell Proliferation Assay kit. The assay is based on the reduction of a tetrazolium salt to a colored formazan by live cells. Briefly, complete media containing DMSO or quercetin and DMSO was removed and replaced with 110 μ l/well of a 1:9 mix of MTS reagent: complete medium; the plate was incubated at 37 $^{\circ}$ C for 180 min; the plate was shaken at 600 rpm for 30 s at room temperature (23 $^{\circ}$ C) and the optical density (OD) at 490 nm was measured for each well using a Multiskan Spectrum plate reader (Thermo Electron Corporation). The average OD of wells without cells was subtracted from the ODs of cell-containing wells. All assays were conducted in triplicates.

Quantification of SARS-CoV-2 RNA

SARS-CoV-2 RNA was extracted from cell culture supernatant using the QIAamp Viral RNA Mini Kit according to the manufacturer's instructions. Viral RNA was

quantified by reverse transcription quantitative PCR (RT-qPCR) using the LightCycler 480 RNA Master Hydrolysis Probes kit and the QuantStudio3 thermal cycler. Primer and probe sequences were specific for the SARS-CoV-2 *E* gene:

forward primer, 5'-ACAGGTACGTTAATAGTTAATAGCGT-3';

reverse primer, 5'-ATATTGCAGCAGTACGCACACA-3'; and.

probe, 5'-FAM-ACACTAGCCATCCTTACTGCGCTTCG-BBQ-3'.

Cycling conditions were as follows: 63 $^{\circ}$ C for 3 min and 95 $^{\circ}$ C for 30 s, followed by 45 cycles of 95 $^{\circ}$ C for 15 s and 60 $^{\circ}$ C for 30 s.

In vitro assay for spike-ACE2 interaction

On a 96-well plate, each well was coated with 50 μ l of 1 μ g/ml of Spike Protein overnight at 4 $^{\circ}$ C; wells were then washed and blocked. Stock solutions of test compounds were prepared: quercetin at 10 mM in DMSO and anti-Spike antibody at 500 nM in PBS. To each well, 10 μ l of diluted test compound and 20 μ l of 1 \times immune buffer (20 mM Tris, 50 mM NaCl, 0.5% NP40, 0.5% sodium deoxycholate, pH 7.5) were mixed and allowed to incubate at room temperature (RT) for 1 h; 20 μ l of ACE2-His (2.5 ng/ μ l) were added and incubation resumed for 1 h; wells were washed three times with immune buffer and blocked with Blocking Buffer 2 for 10 min; 100 μ l of Anti-His-HRP were added to all wells which were incubated for 1 h; wells were emptied, washed three times and blocked before the addition of 100 μ l of freshly prepared HRP chemiluminescent substrates; the luminescence intensity of the samples was measured in a BioTek Synergy 2 microplate reader. The luminescence values in the presence of a test compound were expressed as % of the values obtained in the absence of the compound.

Immunoblotting

For the immunoblotting (IB) experiments, 2.5×10^6 cells in 4 ml of complete medium were seeded in 60 mm plates. After a 24-h incubation, they were transfected, processed, and treated as described above under "Transfection of HEK293 cells". Cell monolayers were washed with PBS; they were scraped off the plates and suspended in 1 ml of PBS; they were rinsed with PBS through two cycles of centrifugation at 1020 *g* for 3 min. Cell pellets were lysed in 50 μ l of IP buffer [PBS, 0.3% n-dodecyl β -D-maltoside (DDM), 20 mM phenylmethylsulfonyl fluoride (PMSF), 1 \times Protease Inhibitor Cocktail (PIC)]; lysates were dispersed through a 30-sec on/30-sec off cycle of sonication in a water bath at 4 $^{\circ}$ C for 3 min at high intensity using a Diagenode sonicator (UCD-200TM). Protein concentrations were determined using the Bio-Rad Bradford Protein Assay kit.

For IB, cell lysates (10 µg) were supplemented with 0.25 volumes of 4× Laemmli Sample Buffer and 0.1 volume of β-mercaptoethanol (final 10% v/v); they were heated at 55 °C for 10 min. Proteins were fractionated on an 8% or 10% SDS-PAGE and electrophoretically transferred onto a polyvinylidene fluoride (PVDF) membrane. The membrane was blocked in Tris-buffered saline (TBS, 50 mM Tris-HCl, 150 mM NaCl, pH 7.6) containing 5% milk-0.1% Tween (blocking solution) for 1 h. It was first incubated overnight at 4 °C with a primary antibody in a 5% bovine serum albumin (BSA) solution and then for 1 h at room temperature, with a horseradish peroxidase (HRP)-conjugated secondary antibody in blocking solution. The membrane was probed for HRP reaction using Bio-Rad Clarity Western ECL Substrate Revelation Kit. Bands were captured using a Bio-Rad ChemiDoc Imaging System and analyzed by densitometry with the Bio-Rad Image Lab Software. The densitometric values for ACE2, Spike-GFP bands were normalized by those for β-actin taken as an internal standard of protein content.

Furin in vitro assay

The assay was conducted using the BPS Bioscience Furin Protease Assay Kit according to the manufacturer's protocol. Briefly, a 50-µl reaction mixture in 25 mM Tris/1 mM CaCl₂ 0.5% w/v Brij-35, pH 9.0 (assay buffer) was prepared with 50 ng of recombinant soluble human furin, 10 µl of quercetin at different concentrations in 10% DMSO (1% final); the mixture was kept at room temperature for 30 min; it was then supplemented with 50 µl of 4 µM of the furin substrate PyroGlu-Arg-Thr-Lys-Arg-4 methylcoumaryl-7-amide (Pyr-RTKR-AMC) in the assay buffer, and further incubated for 30 min at room temperature. Fluorescence intensity resulting from substrate cleavage was measured at an excitation of 380 nm and an emission of 460 nm using a Tecan Infinite M1000 microplate reader. Quercetin inhibitory activity is expressed in % relative to blank (100%). Decanoyl-Arg-Val-Lys-Arg-chloromethylketone (Dec-RVKR-CMK), a confirmed furin inhibitor, was used as a positive control of inhibition.

Statistical analysis

Quantitative values are expressed as means ± standard deviation (SD). They were calculated and statistically compared by one-way ANOVA using GraphPad Prism version 9.5.1. Significance of differences between experimental groups was set at $p < 0.05$.

Results

Quercetin inhibits SARS-CoV-2 infection of VeroE6 and Caco2 cells

To determine whether quercetin could inhibit virus infection, Vero E6 and Caco-2 cells were infected with

SARS-CoV-2 and treated with quercetin at different concentrations ranging from 6.25 µM to 400 µM. Two days post-infection (dpi), supernatants were collected, and viral RNA was quantified by RT-qPCR. The Ct values increased with increasing concentrations of quercetin, reflecting a decrease in viral genomes released, i.e., an inhibition of virion production. The half inhibitory concentration (IC₅₀) of the inhibition in Vero E6 and Caco-2 cells was 166.6 µM (Fig. 1A) and 145.2 µM (Fig. 1B), respectively.

The titer of infectious particles in culture supernatants following quercetin treatment of infected cells was assessed by determining their TCID₅₀/ml: it was 229 µM and 341.8 µM for Vero E6 (Fig. 1C) and Caco-2 (Fig. 1D) cells, respectively.

The quercetin concentrations tested did not induce any significant loss of viability of either cell type, giving a half cytotoxic concentration (CC₅₀) > 400 µM (Fig. 1, E and F), and a Selectivity Index (SI, CC₅₀/IC₅₀) of > 2.4.

Quercetin inhibits the formation of syncytia by S and ACE2 co-expressing cells

Since some of quercetin bioactivities has been ascribed to its disturbance of the cellular membrane lipid bilayer by intercalating into it [26, 27], we surmised that this intercalation might impair not only the interaction between the viral S protein and cellular ACE2, but also the topology and activity of membrane receptors and enzymes which facilitate membrane fusion and viral entry. We therefore set up a HEK293 cell-based assay (without infectious virus) to examine the effect of quercetin on syncytium formation that results from S protein-ACE2 interaction.

When HEK293 cells were transfected with the pS-GFP or the pACE2 plasmid vector, cell monolayers preserved their normal spread-out morphology as visible by bright-field microscopy (Fig. 2A, a, b). Addition of 400 µM to pACE2-transfected cells or untransfected did not alter this morphology (Fig. 2A, c, d). When, on the other hand, cells were transfected with both pS-GFP and the pACE2 vectors [heretofore named HEK293(S+ACE2) cells], the monolayer was characterized by groupings of cells around denuded areas, suggesting the formation of syncytia (Fig. 2A, e). Addition of quercetin (100 to 400 µM) gradually restored the normal morphology of monolayers (Fig. 2A f-h). This was confirmed by examining the distribution of GFP fluorescence (Fig. 2B). When S-GFP was expressed alone, punctate fluorescent cells were observed around the plate (Fig. 2B, h). With HEK293(S+ACE2) cells, intense fluorescence surrounding dark areas were observed (Fig. 2B, a). In the presence of increasing concentrations of quercetin, the fluorescence intensity gradually decreased and became punctate again (Fig. 2B, b-g).

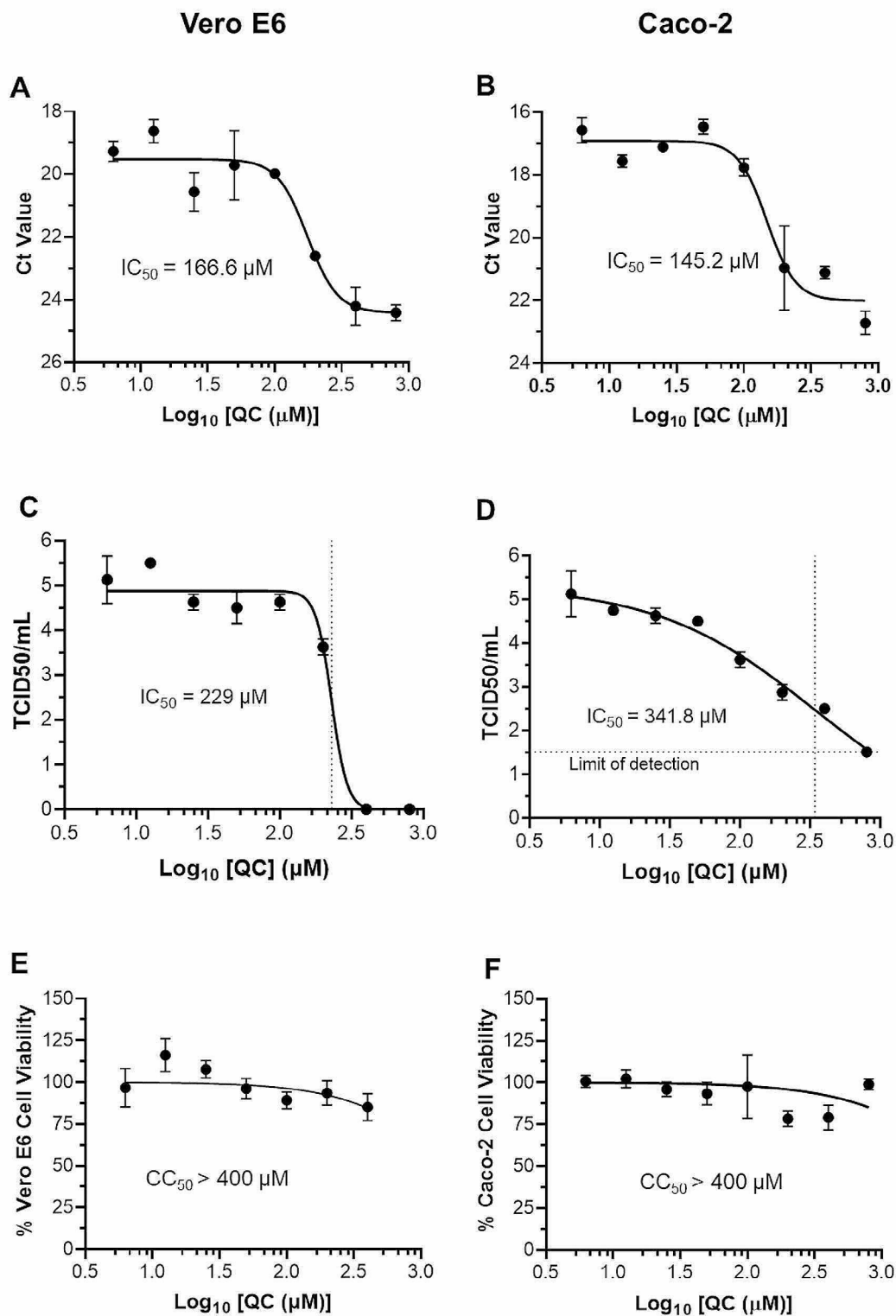


Fig. 1 Quercetin inhibits SARS-CoV-2 infection. Vero E6 (A) or Caco2 (B) cells were pre-treated with various concentrations of quercetin (ranging from 6.25 μM to 400 μM) before being infected with SARS-CoV-2 at an MOI of 0.1. Supernatants were harvested after 48 h, and virus RNA was quantified via RT-qPCR. RNA levels are expressed on an inverse y-axis as Ct (cycle threshold) values. Results were obtained from three independent experiments and are expressed as mean Ct values \pm SD (C and D). Cell viability after 48 h incubation with quercetin in the same concentration range was determined for Vero E6 (E) and Caco2 (F) cells using the CyQUANT™ XTT Cell Viability Assay kit

The syncytialization of HEK293(S+ACE2) cells was ascertained by confocal microscopy. As shown in Fig. 2C, a, areas of intense GFP fluorescence were characterized by clusters of blue-stained nuclei, as can be expected of syncytia (arrows). The clusters gradually decreased in number and fluorescence intensity with the addition of increasing concentrations of quercetin (Fig. 2C, b-f). Such clusters were not observed when cells were pS-GFP or pACE2 alone (Fig. 2C, g-h)

Quercetin IC_{50} of syncytialization of HEK293(S+ACE2) cells, CC_{50} of HEK293 cells, and IC_{50} of in vitro binding of ACE2 to S-RBD

Since GFP fluorescence intensity correlated with the abundance of syncytia, its integrated intensity per image was measured and used to derive a IC_{50} of quercetin: it was found to be 156.7 μ M (Fig. 3A). In a separate experiment, MTS viability assay was applied to HEK293 cells in the same concentration range to derive a CC_{50} of quercetin: it was above the highest concentration tested (>400 μ M, Fig. 3B).

Syncytialisation inhibition could be due to quercetin interference in the binding of the viral Spike protein to cellular ACE2 as inferred from *in silico* docking studies [15, 16]. We examined this possibility in an in-vitro assay of binding of Spike protein receptor-binding domain (RBD) to recombinant ACE2. Quercetin up to 300 μ M failed to inhibit this binding (Fig. 3C) whereas an anti-S antibody very efficiently did so (Fig. 3D).

Quercetin inhibits the production of the S2' fragment of the spike protein

The S-GFP expressed is the transmembrane spike protein C-terminally fused to GFP (Fig. 4A). In immunoblotting of extracts of HEK293 cells expressing the fusion protein, an anti-GFP antibody should recognize the S protein as well as membrane-bound N-terminally cleaved products, most prominently membrane-bound S2 and S2'. This was indeed the case, as shown in Fig. 4B, (lane 8). The identity of the immune bands was confirmed via immunoblotting cell lysates from cells transfected with a vector for producing unfused S protein or S-GFP fusion protein, using two different polyclonal antibodies raised against the native S (Supplementary Fig. S1).

In HEK293(S+ACE2) cells, expression of S and its processed fragments was consistently less robust compared to cells expressing S-GFP alone (complemented with an empty vector to equalize the total amount of vector DNA; Fig. 4B, a, lane 2 vs. lane 8). The addition of quercetin to the doubly transfected cells reduced the expression of all these S forms in a concentration-dependent manner (Fig. 4B, a, lanes 2–7).

ACE2 expression in HEK293(S+ACE2) cells was similarly affected by the double transfection (Fig. 4B, b, lane 2

vs. lane 9) and quercetin addition (Fig. 4B, b, lanes 2–7). Shed ACE2 in spent media was titrated by ELISA: the decrease in media paralleled that in cells (not shown), suggesting that quercetin did not affect shedding in any way.

The optical density of immunoreactive bands corresponding to S, S2, S2', ACE2 was measured and normalized relative to that of β -actin (Fig. 4C). The quercetin-induced decrease in S and S2 expression did not reach significance (Fig. 4C, a-b); however, the decrease in S2' expression at 100 μ M quercetin and above was significant (Fig. 4C, c).

S2 and S2' are generated through cleavage by furin after specific basic motifs [28]. S2/S and S2'/S2 ratio were computed from their normalized values to assess the effect of quercetin on these two major proteolytic events. A significant decrease in the conversion of S2 to S2' was noted at 200 and 400 μ M (Fig. 4C, e). This conversion exposes an N-terminal hydrophobic motif called fusion peptide (FP, in Fig. 4A) which facilitates fusion among cells.

Extracts of HEK293(S+ACE2) cells were subjected to immunoprecipitation with an anti-GFP antibody and the precipitates subjected to immunoblotting using either the anti-GFP antibody or an anti-ACE2 antibody. The results showed that addition of quercetin did not significantly change the ratio of S or S2 to ACE2 pulled down by the antibody (Supplemental Fig. S2), suggesting that the flavonol did not interfere with binding between the two molecules, in concordance with the results of the in vitro binding assay using recombinant S-RBD and ACE2 (see Fig. 3C).

Quercetin inhibits furin in vitro

Zhu and coll. have examined the inhibitory effect of several polyphenols, including quercetin, on furin proteolysis of its fluorogenic substrate Pyr-RTKR-AMC, in the concentration range of 0 to 40 μ M: they found that quercetin inhibited this activity by about 45% at 40 μ M [18]. Using a similar in vitro furin assay and extending the concentration range (0 to 300 μ M), we determined the IC_{50} of inhibition to be about 116 μ M (Fig. 5A). The IC_{50} of Dec-RVKR-CMK canonical furin inhibitor was 7.7 nM under the same conditions (Fig. 5B), suggesting that inhibition by quercetin may be through mechanism not involving interaction with the furin catalytic site.

Discussion

This study demonstrates that quercetin, at concentrations above 100 μ M can inhibit SARS-CoV-2 infection of Vero E6 and Caco-2 cells. The term 'infection' refers broadly to any step of the virus life cycle — including attachment, entry, genome replication, gene transcription, assembly, and egress — all of which are necessary for the production of infectious progeny virions. Quantification of the

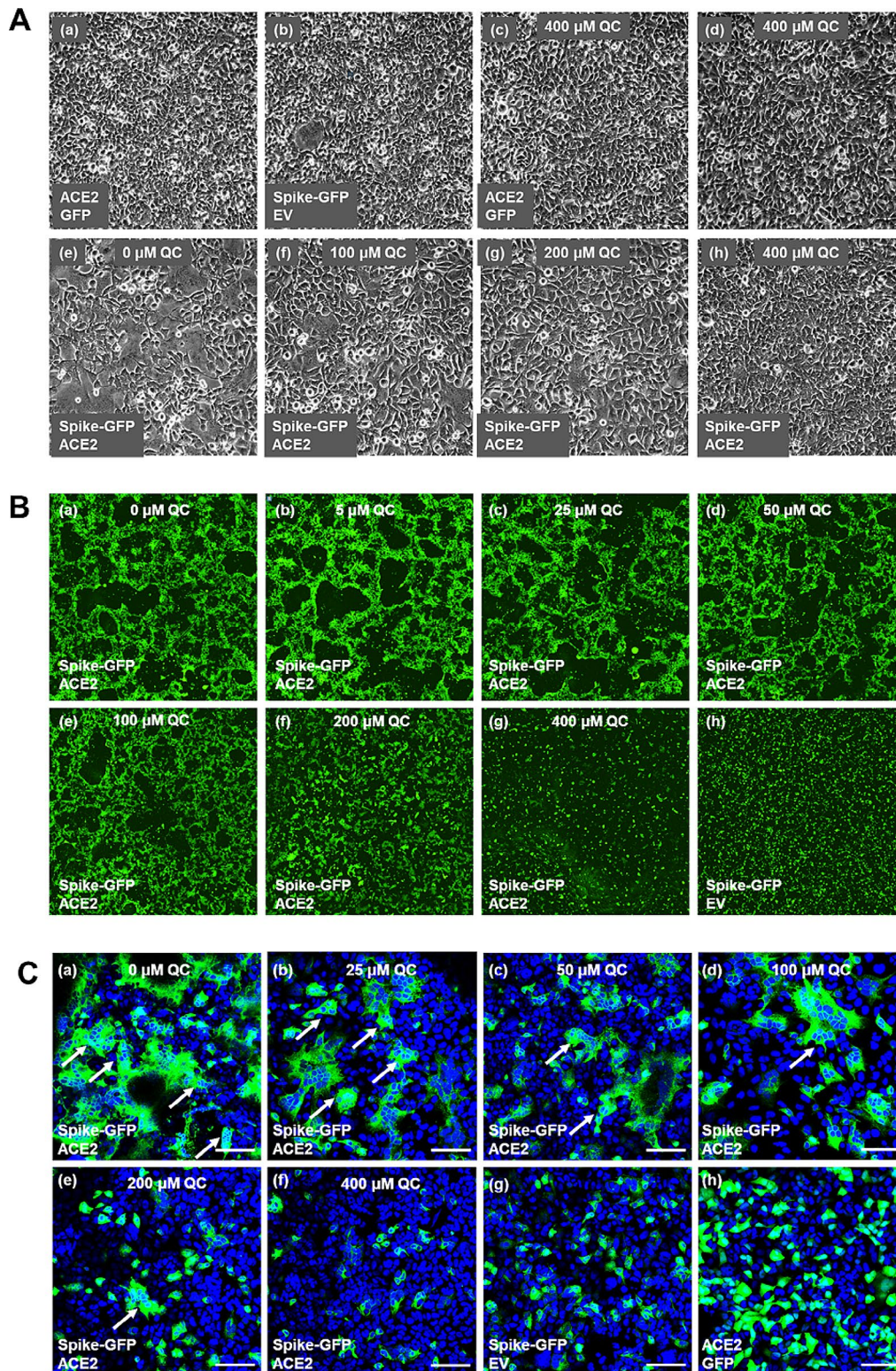


Fig. 2 Microscopy of HEK293(S+ACE2) cell syncytialization and its inhibition by quercetin. **(A)** Brightfield microscopy. Controls cells (a-d) were transfected with plasmid vector for expression of indicated proteins and later cultured for 20 h in medium containing either DMSO (a, b) or 400 μM quercetin in DMSO. Experimental HEK293(S+ACE2) cells (e-h) were cultured for 20 h in medium containing either DMSO (e) or the indicated concentrations of quercetin (f-h). **(B)** Fluorescence microscopy. Control and experimental cells were treated as in A; GFP fluorescence was camera-captured in the Incucyte. **(C)** Confocal microscopy. Controls and experimental cells were treated as A, fixed, and stained with Hoechst. Images were captured. Arrows point to clusters of nuclei within region intense GFP fluorescence. Scale bar: 100 μm

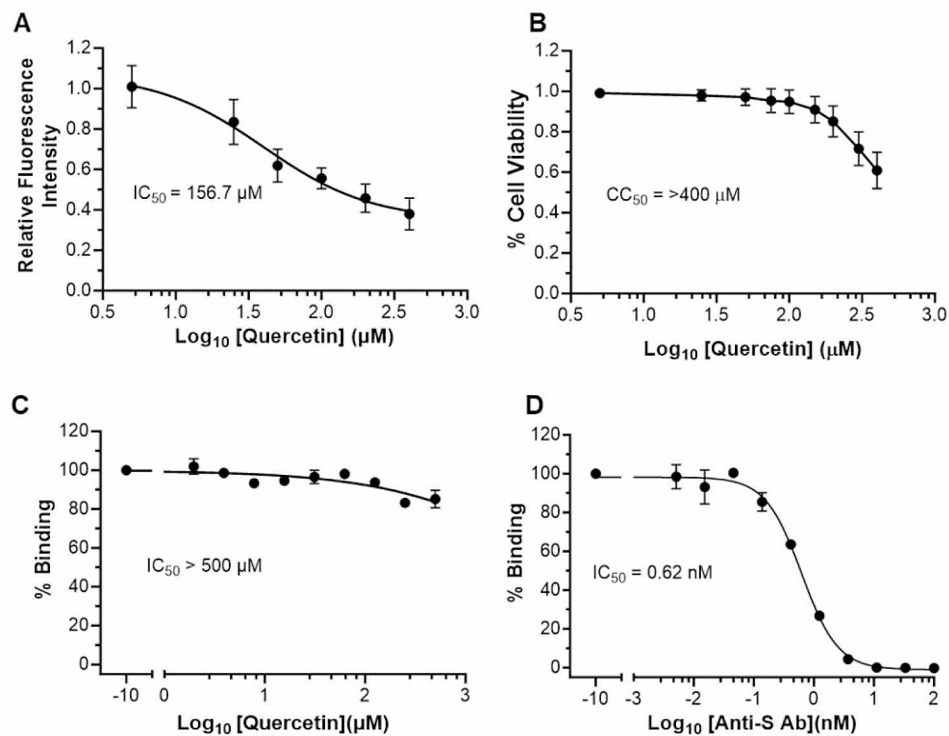


Fig. 3 Quercetin IC₅₀ and CC₅₀. **(A)** IC₅₀ of quercetin inhibition of syncytialization of HEK293(S+ACE2) based on decrease of GFP fluorescence. **(B)** CC₅₀ of quercetin on HEK293 cells as determined using the MTS viability assay. **(C)** IC₅₀ of quercetin inhibition of in vitro binding of ACE2 to Spike RBD. **(D)** IC₅₀ of anti-Spike antibody inhibition of in vitro binding of ACE2 to Spike RBD. Results are from 3 separate experiments and are expressed as means ± SD

levels of virus genomic RNA was used as a surrogate measure of virus replication. Their reduction in the presence quercetin suggests that cell exposure to this flavonol negatively impacts virus replication.

These effective concentrations of quercetin in this study are 2-order of magnitude above those ordinarily found in blood following oral administration of quercetin to animals or humans [29], putting into question the ability of this flavonol to block infection by the virus in vivo. However, a few studies have shown that lungs, the tissues primarily infected by SARS-CoV-2, were among the organs where quercetin and its metabolites mostly accumulated after such an administration [30, 31]. Moreover, experimental evaluation of antiviral activity of green tea extracts in mice and humans have provided evidence that concentrations of epigallocatechin 3-0 gallate (EGCG), the active phytochemical and a polyphenol like quercetin, could reach and surpass 100 μM in saliva or pharyngeal swabs, 3 min to 2 h after oral administration [32–34], raising the possibility that the upper respiratory tract could similarly accumulate quercetin with the choice of a proper mode of administration (e.g. oral or nasal spray).

In this study, the IC₅₀ of quercetin inhibition of SARS-CoV-2 replication in Vero E6 and Caco2 cells was about 150 μM as determined by RT-qPCR of viral RNA released in the medium. In contrast, Kandeil et al. [35] reported that the flavonol inhibited SARS-CoV-2 infection of

Vero E6 with an IC₅₀ of 18.2 μM, as assessed by a plaque reduction assay. Using human lung epithelial Calu-3 for infection and a similar Vero E6 cell-based plaque-forming assay, Chaves et al. [36] determined the IC₅₀ of quercetin inhibition to be 2.4 μM. This discordance in IC₅₀ results could be explained by differences of viral strain, cell line, and MOI used for infection, among other factors.

The binding of SARS-CoV-2 Spike protein to human ACE2 is the prelude to viral entry into and infection of human cells. When the S protein is newly biosynthesized within the infected cells, it is translocated to the plasma membrane where it interacts with the ACE2 of adjacent cells, initiating the formation of syncytia [37]. Both S and ACE2 are type-1 transmembrane proteins; both can be susceptible to proteolytic cleavages by membrane proteases, releasing the N-terminal fragment into the extracellular space. Furin and TMPRSS2 mediate this endoproteolysis: furin is the primary enzyme that converts S to N-terminal S1 and transmembrane S2 proteins, and of the latter to transmembrane S2' protein; whereas TMPRSS2 mediates the shedding of the ACE2 ectodomain following its binding to the S protein [28]. The N-terminal hydrophobic FP of S2' promotes membrane fusion and syncytium formation [38]. The orchestration of these proteolytic events may explain the apparent lower level of both S and ACE2 when they are co-expressed in HEK293 cells compared to when either

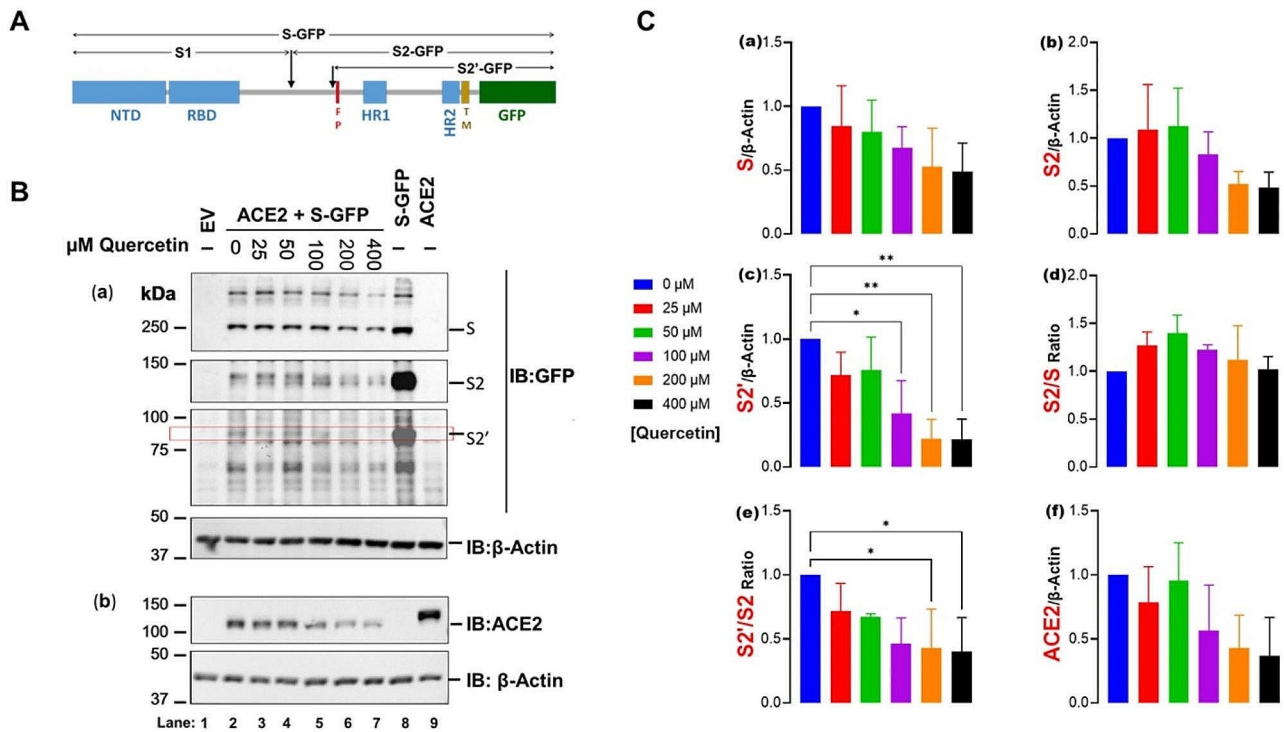


Fig. 4 Immunoblotting of ACE2 as well as S and S-related proteins in HEK293(S+ACE2) cells treated with quercetin. **(A)** Diagrammatic representation of the S-GFP fusion protein and its proteolytic fragment. Acronyms: NTD, N-terminal domain; RBD, receptor binding domain; FP, fusion peptide; HR, heptad region, TM, transmembrane domain, GFP, green fluorescent protein. **(B)** Representative Immunoblot of cells extracts transfected with empty vector (EV) (lane 1), vector for expression of S-GFP (lane 8), ACE2 (lane 9), or both S-GFP and ACE2 (lanes 2–7) with DMSO (lane 2) or increasing concentrations of quercetin (lanes 3–7); (a) The blot was immuno-probed successively for GFP and β-actin; (b) a parallel blot of the same cell extracts was immune-probed successively for ACE2 and β-actin antibody. **(C)** Densitometry of immunoreactive bands in three separate experiments was conducted. S, S2 and S2' and ACE2 values were normalized by those of β-actin (a–c, f). The ratios S2/S (d) and S2'/S2 (e) were computed as measures of the proteolytic conversion S to S2 and S2 to S2', respectively. Values are expressed as means ± SD. * < 0.05, ** < 0.005

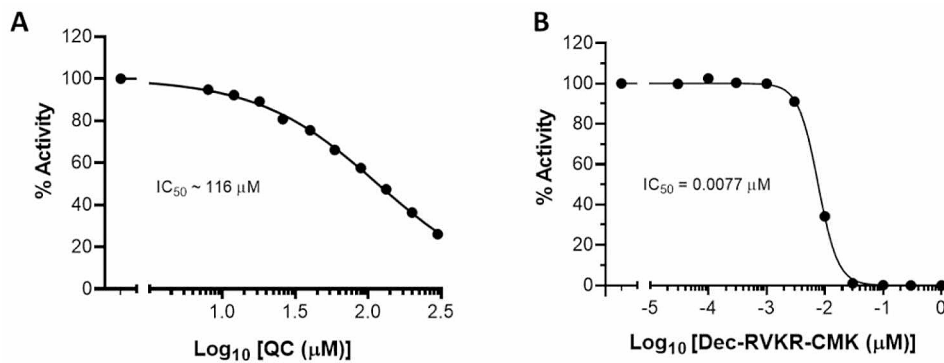


Fig. 5 Quercetin inhibition of furin activity. As described under Materials and Methods, furin proteolysis of the fluorogenic Pyr-RTKR-AMC substrate was assayed in absence or the presence of increasing concentrations of: **(A)** quercetin or **(B)** the synthetic Dec-RVKR-CMK inhibitor

protein is expressed alone. A decrease in endogenous ACE2 expression following transfection of SARS-CoV-2 spike protein has also been noted in Vero E6 cells [39].

Addition of quercetin at 100 to 400 mM interferes with syncytium formation by HEK293(S+ACE2) cells. This inhibition occurs with an IC_{50} of 156.7 μM. In contrast, using HEK293-III A cells expressing S and ACE2, Singh et al. [39] reported that quercetin at 10 μM significantly

reduced the size (by ~80%) and area (by ~60%) of syncytia, as determined by brightfield image analysis. Why syncytialization inhibition by the flavonol appears to be greater in this cell line compared to the one used in this study is unclear. Like its effect on apoptosis [40], the IC_{50} of quercetin inhibition of syncytium formation can significantly vary among cell lines.

Quercetin addition to HEK293(S+ACE2) cells had little effect on the conversion of S to S2, but it significantly reduced the conversion of S2 to S2', suggesting it inhibited the enzyme(s) responsible. Furin is one of the enzymes mediating this conversion [28]. We found that quercetin inhibits furin cleavage of a specific synthetic substrate *in vitro*, in a concentration-dependent manner and with an IC₅₀ of 116 μM. This IC₅₀ value is not far removed from that obtained in HEK293(S+ACE2) syncytialization assay (156.7 μM) as well as those obtained in the SARS-CoV-2 infectivity assay with Vero E6 (166.6 μM) or Caco2 (145.2 μM) cells. In this context, it is worth mentioning that *in vitro* inhibition of furin by polyphenols has been attributed, not to inactivation of its catalytic site, but to the formation of quinone oxidation products that interact non-specifically with the furin protein, changing its conformation and reducing its enzymatic activity [41].

It is also possible that the intercalation of quercetin into the lipid bilayer perturbs the topology of membrane enzymes [42], preventing the binding of S2 protein to the catalytic pocket of furin. Interestingly, quercetin-3-glucoside—also known as isoquercetin or isoquercitrin—which is less hydrophobic than quercetin, and thus less membrane-intercalating, failed to inhibit syncytium formation (Supplemental Fig. S3).

Conclusion

Data presented in this report indicate that quercetin can inhibit SARS-CoV-2 replication in Vero E6 and Caco-2 cells. Results from experiments with surrogate HEK293(S+ACE2) cells suggest that, mechanistically, it prevents the syncytium formation which normally follows initial expression of viral proteins in infected cells, facilitating virion propagation. At the molecular level, quercetin reduction of furin-mediated production of the S2' fusogenic fragment might contribute to the diminished syncytialization. The inhibition of syncytium formation and of S2' fragment production observed in the surrogate HEK293 (S+ACE2) cells remains to be demonstrated in virus-infected cells. Nonetheless, the present data support the possibility that quercetin could be an anti-COVID-19 drug. Its *in vivo* efficacy should be evaluated experimentally on appropriate animal models and, ultimately, in clinical trials on human patients.

Abbreviations

3CL ^{pro}	3-Chymotrypsin-like protease
ACE2	Angiotensin-converting enzyme 2
ANOVA	Analysis of variance
BSA	Bovine fetal albumin
CatB	Cathepsin B
CatL	Cathepsin L
COVID-19	Coronavirus disease of 2019
DDM	n-Dodecyl-β-D-maltoside
DMEM	Dulbecco's Modified Eagle Medium
DMSO	Dimethylsulfoxide
DPI	Days post-infection

eGFP	Enhanced GFP
EV	Empty vector
FBS	Fetal bovine serum
FP	Fusion peptide
GFP	Green fluorescent protein
HEK	Human embryonic kidney
HRP	Horseradish peroxidase
IB	Immunoblotting
IP	Immunoprecipitation
MEM	Minimal Essential Medium
MOI	Multiplicity of infection
M ^{pro}	Main protease
NML	National Microbiology Laboratory
OD	Optical density
PBS	Phosphate-buffered saline
PHAC	Public Health Agency of Canada
PIC	Protease inhibitor cocktail
PL ^{pro}	Papain-like protease
PMSF	Phenylmethylsulfonyl fluoride
PVDFv	Polyvinylidene difluoride
QC	Quercetin
RBD	Receptor binding domain
RdRp	RNA-dependent RNA polymerase
RT-qPCR	Reverse transcription-polymerase chain reaction
SARS-CoV-2	Severe acute respiratory syndrome-coronavirus 2
SD	Standard deviation
TBS	Tris-buffered saline
TMPRSS2	transmembrane protease serine 2

Supplementary Information

The online version contains supplementary material available at <https://doi.org/10.1186/s12985-024-02299-w>.

Supplementary Material 1: Supplementary Figure S1. Confirmation of S protein bands. Cells were transfected with the indicated expression vectors and their extracts analyzed as described for Fig. 3. Immunoblotting of S protein and its fragments was performed using antibodies from Abcam (cat# ab272504) and Sino Biological (cat# 40592-T62). The Spike-Linker-GFP gene is expressed as a fusion S-GFP protein whereas with the Spike-P2A-GFP gene, the S protein and GFP are expressed as two separate molecules, hence the size difference in immunoreactive S bands produced per the two vectors.

Supplementary Material 2: Supplementary Figure S2. Pull-down of ACE2 by S protein. HEK293(S+ACE2) cell extracts were subjected to immunoprecipitation with GFP-trap beads. The precipitates were analyzed by immunoblotting for ACE-2 and GFP; the densities of immunoreactive bands were determined. A. A representative blot. B&C. The S/ACE2 and S2/ACE density ratios were computed. The values (means ± SD of 3 independent experiments) of quercetin-treated cells were expressed relative to those of DMSO treated control cells.

Supplementary Material 3: Supplementary Figure S3. Effect of isoquercetin on HEK293(S+ACE2) syncytialization. The experiment was conducted as described in Fig. 1. Isoquercetin did not inhibit the formation of syncytia.

Supplementary Material 4: Supplementary Table S1. List of reagents, sources and catalog numbers

Supplementary Material 5: Supplementary Materials and Methods

Acknowledgements

Not applicable.

Author contributions

These authors conducted the experiments and analyzed the data (AR, MChA, LB, SH, WZ), designed the study (MM, LB, MChr), wrote the manuscript (MM) and reviewed the manuscript (all the authors).

Funding

This research was funded by grants from the Richard and Edith Strauss Foundation, the Lazaridis Family Foundation, Power Corporation, the Fondation J-Louis Lévesque, and la Fondation Notre Dame de Zeitoun. This work was also supported in part by the Public Health Agency of Canada.

Data availability

No datasets were generated or analysed during the current study.

Declarations

Ethics approval and consent to participate

Not applicable.

Consent for publication

Not applicable.

Competing interests

The authors declare no competing interests.

Received: 20 November 2023 / Accepted: 18 January 2024

Published online: 25 January 2024

References

- Msemburi W, Karlinsky A, Knutson V, Aleshin-Guendel S, Chatterji S, Wakefield J. The WHO estimates of excess mortality associated with the COVID-19 pandemic. *Nature*. 2023;613:130–7.
- Harrison AG, Lin T, Wang P. Mechanisms of SARS-CoV-2 transmission and pathogenesis. *Trends Immunol*. 2020;41:1100–15.
- Horita N, Fukumoto T. Global case fatality rate from COVID-19 has decreased by 96.8% during 2.5 years of the pandemic. *J Med Virol*. 2023;95:e28231.
- Ganguli S, Howlader S, Dey K, Barua S, Islam MN, Aquib TI, Partho PB, Chakraborty RR, Barua B, Howlader MDH, Biswas PK. Association of comorbidities with the COVID-19 severity and hospitalization: a study among the recovered individuals in Bangladesh. *Int J Health Sci*. 2022;16:30–45.
- Pandey R, Rai D, Tahir MW, Wahab A, Bandyopadhyay D, Lesho E, Laguio-Vila M, Fentanes E, Tariq R, Naidu SS, Aronow WS. Prevalence of comorbidities and symptoms stratified by severity of illness amongst adult patients with COVID-19: a systematic review. *Arch Med Sci Atheroscler Dis*. 2022;7:e5–e23.
- Ning C, Wang H, Wu J, Chen Q, Pei H, Gao H. The COVID-19 vaccination and vaccine inequity worldwide: an empirical study based on global data. *Int J Environ Res Public Health*. 2022;19.
- Sun G, Sui Y, Zhou Y, Ya J, Yuan C, Jiang L, Huang M. Structural basis of covalent inhibitory mechanism of TMPRSS2-related serine proteases by camostat. *J Virol*. 2021;95:e0086121.
- Gunst JD, Staerke NB, Pahus MH, Kristensen LH, Bodilsen J, Lohse N, Dalgaard LS, Bronnum D, Frobert O, Honge B, et al. Efficacy of the TMPRSS2 inhibitor camostat mesilate in patients hospitalized with Covid-19—a double-blind randomized controlled trial. *EclinicalMedicine*. 2021;35:100849.
- Yuan Z, Pavel MA, Wang H, Kwachukwu JC, Mediouni S, Jablonski JA, Nettles KW, Reddy CB, Valente ST, Hansen SB. Hydroxychloroquine blocks SARS-CoV-2 entry into the endocytic pathway in mammalian cell culture. *Commun Biol*. 2022;5:958.
- García-Albeniz X, Del Amo J, Polo R, Morales-Asencio JM, Hernan MA. Systematic review and meta-analysis of randomized trials of hydroxychloroquine for the prevention of COVID-19. *Eur J Epidemiol*. 2022;37:789–96.
- Marzi M, Vakil MK, Bahmanyar M, Zarenezhad E. Paxlovid: mechanism of action, synthesis, and in silico study. *BioMed Res Int*. 2022;2022:7341493.
- Konwar M, Maurya M, Bose D. A meta-analysis of safety of different regimens of remdesivir in COVID-19 patients. *Curr Drug Saf*. 2022;17:158–67.
- Babadaei MMN, Hasan A, Vahdani Y, Bloukh SH, Sharifi M, Kachooei E, Haghighat S, Falahati M. Development of remdesivir repositioning as a nucleotide analog against COVID-19 RNA dependent RNA polymerase. *J Biomol Struct Dyn*. 2021;39:3771–9.
- Najjar-Debbiny R, Gronich N, Weber G, Khoury J, Amar M, Stein N, Goldstein LH, Saliba W. Effectiveness of paxlovid in reducing severe coronavirus disease 2019 and mortality in high-risk patients. *Clin Infect Dis*. 2023;76:e342–9.
- Hiremath S, Kumar HDV, Nandan M, Mantesh M, Shankarappa KS, Venkataravanappa V, Basha CRJ, Reddy CNL. In silico docking analysis revealed the potential of phytochemicals present in *Phyllanthus amarus* and *Andropogon paniculata*, used in Ayurveda medicine in inhibiting SARS-CoV-2. *Biotech*. 2021;11:44.
- Pan B, Fang S, Zhang J, Pan Y, Liu H, Wang Y, Li M, Liu L. Chinese herbal compounds against SARS-CoV-2: Puerarin and quercetin impair the binding of viral S-protein to ACE2 receptor. *Comput Struct Biotechnol J*. 2020;18:3518–27.
- Manjunathan R, Periyaswami V, Mitra K, Rosita AS, Pandya M, Selvaraj J, Ravi L, Devarajan N, Doble M. Molecular docking analysis reveals the functional inhibitory effect of Genistein and Quercetin on TMPRSS2: SARS-CoV-2 cell entry facilitator spike protein. *BMC Bioinform*. 2022;23:180.
- Zhu J, Declercq J, Creemers JW, Chen C, Cui Y, Van de Ven WJ, Vermorken AJ. Limitations of inhibitory activities of polyphenols on furin-mediated substrate processing. *Curr Med Chem*. 2012;19:3641–50.
- Liu X, Raghuvanshi R, Ceylan FD, Bolling BW. Quercetin and its metabolites inhibit recombinant human angiotensin-converting enzyme 2 (ACE2) activity. *J Agric Food Chem*. 2020;68:13982–9.
- Abian O, Ortega-Alarcon D, Jimenez-Alesanco A, Ceballos-Laita L, Vega S, Reyburn HT, Rizzuti B, Velazquez-Campoy A. Structural stability of SARS-CoV-2 3CLpro and identification of quercetin as an inhibitor by experimental screening. *Int J Biol Macromol*. 2020;164:1693–703.
- Zhu Y, Scholle F, Kisthardt SC, Xie DY. Flavonols and dihydroflavonols inhibit the main protease activity of SARS-CoV-2 and the replication of human coronavirus 229E. *Virology*. 2022;571:21–33.
- Munafa F, Donati E, Brindani N, Ottonello G, Armirotti A, De Vivo M. Quercetin and luteolin are single-digit micromolar inhibitors of the SARS-CoV-2 RNA-dependent RNA polymerase. *Sci Rep*. 2022;12:10571.
- Yang D, Wang T, Long M, Li P, Quercetin. Its main pharmacological activity and potential application in clinical medicine. *Oxid Med Cell Longev*. 2020;2020:8825387.
- Fodor A, Tipericiu B, Login C, Orasan OH, Lazar AL, Buchman C, Hanghiceal P, Sitar-Taut A, Suharoschi R, Vulturar R, Cozma A. Endothelial dysfunction, inflammation, and oxidative stress in COVID-19—mechanisms and therapeutic targets. *Oxid Med Cell Longev*. 2021;2021:8671713.
- Donnelly MLL, Luke G, Mehrotra A, Li X, Hughes LE, Gani D, Ryan MD. Analysis of the aphthovirus 2A/2B polyprotein 'cleavage' mechanism indicates not a proteolytic reaction, but a novel translational effect: a putative ribosomal 'skip'. *J Gen Virol*. 2001;82:1013–25.
- Tsuchiya H. Structure-dependent membrane interaction of flavonoids associated with their bioactivity. *Food Chem*. 2010;120:1089–96.
- Tsuchiya H. Membrane interactions of phytochemicals as their molecular mechanism applicable to the discovery of drug leads from plants. *Molecules*. 2015;20:18923–66.
- Essalmani R, Jain J, Susan-Resiga D, Andreo U, Evagelidis A, Derbali RM, Huynh DN, Dallaire F, Laporte M, Delpal A, et al. Distinctive roles of furin and TMPRSS2 in SARS-CoV-2 infectivity. *J Virol*. 2022;96:e0012822.
- Carullo G, Badolato M, Aiello F. Bioavailability and biochemistry of quercetin and applications to health and diseases. *Polyphenols: mechanisms of action in human health and disease*. Elsevier; 2018. pp. 361–71.
- Paulke A, Eckert GP, Schubert-Zsilavecz M, Wurglics M. Isoquercitrin provides better bioavailability than quercetin: comparison of quercetin metabolites in body tissue and brain sections after six days administration of isoquercitrin and quercetin. *Pharmazie*. 2012;67:991–6.
- de Boer VC, Dihal AA, van der Woude H, Arts IC, Wolfram S, Alink GM, Rietjens IM, Keijer J, Hollman PC. Tissue distribution of quercetin in rats and pigs. *J Nutr*. 2005;135:1718–25.
- Furushima D, Otake Y, Koike N, Onishi S, Mori T, Ota N, Yamada H. Investigation of the oral Retention of Tea catechins in humans: an exploratory interventional study. *Nutrients*. 2021;13.
- Onishi S, Mori T, Kanbara H, Habe T, Ota N, Kurebayashi Y, Suzuki T. Green tea catechins adsorbed on the murine pharyngeal mucosa reduce influenza A virus infection. *J Funct Foods*. 2020;68:103894.
- Zhang Z, Hao M, Zhang X, He Y, Chen X, Taylor EW, Zhang J. Potential of green tea EGCG in neutralizing SARS-CoV-2 Omicron variant with greater tropism toward the upper respiratory tract. *Trends Food Sci Technol*. 2023;132:40–53.
- Kandeil A, Mostafa A, Kutkat O, Moatasim Y, Al-Karmalawy AA, Rashad AA, Kayed AE, Kayed AE, El-Shesheny R, Kayali G, Ali MA. Bioactive polyphenolic compounds showing strong antiviral activities against severe acute respiratory syndrome coronavirus 2. *Pathogens*. 2021;10.
- Chaves OA, Fintelman-Rodrigues N, Wang X, Sacramento CQ, Temerozo JR, Ferreira AC, Mattos M, Pereira-Dutra F, Bozza PT, Castro-Faria-Neto HC et

- al. Commercially available flavonols are better SARS-CoV-2 inhibitors than isoflavone and Flavones. *Viruses*. 2022;14.
37. Buchrieser J, Dufloo J, Hubert M, Monel B, Planas D, Rajah MM, Planchais C, Porrot F, Guivel-Benhassine F, Van der Werf S, et al. Syncytia formation by SARS-CoV-2-infected cells. *EMBO J*. 2021;40:e107405.
38. Schaefer SL, Jung H, Hummer G. Binding of SARS-CoV-2 fusion peptide to host endosome and plasma membrane. *J Phys Chem B*. 2021;125:7732–41.
39. Singh RD, Barry MA, Croatt AJ, Ackerman AW, Grande JP, Diaz RM, Vile RG, Agarwal A, Nath KA. The spike protein of SARS-CoV-2 induces heme oxygenase-1: pathophysiologic implications. *Biochim Biophys Acta - Mol Basis Dis*. 2022;1868:166322.
40. Hashemzaei M, Delarami Far A, Yari A, Heravi RE, Tabrizian K, Taghdisi SM, Sadegh SE, Tsarouhas K, Kouretas D, Tzanakakis G, et al. Anticancer and apoptosis-inducing effects of quercetin in vitro and in vivo. *Oncol Rep*. 2017;38:819–28.
41. Zhu J, Van de Ven WJ, Verbiest T, Koeckelberghs G, Chen C, Cui Y, Vermorken AJ. Polyphenols can inhibit furin in vitro as a result of the reactivity of their auto-oxidation products to proteins. *Curr Med Chem*. 2013;20:840–50.
42. de Granada-Flor A, Sousa C, Filipe HAL, Santos M, de Almeida RFM. Quercetin dual interaction at the membrane level. *ChemComm*. 2019;55:1750–3.

Publisher's Note

Springer Nature remains neutral with regard to jurisdictional claims in published maps and institutional affiliations.